Journal of the Mechanical Behavior of Biomedical Materials 75 (2017) 330–335

Contents lists available at ScienceDirect

Journal of the Mechanical Behavior of Biomedical Materials

journal homepage: www.elsevier.com/locate/jmbbm

Biomechanics of human parietal pleura in uniaxial extension

Luis E. Morales Tenorio[a,b], Kelsey J. Devine[a], Jayme Lee[c], Timothy M. Kowalewski[c], Victor H. Barocas[a,*]

[a] Dept. of Biomedical Engineering, University of Minnesota, Minneapolis, MN 55455, USA
[b] Dept. of Urology, University of Minnesota - Medical School, Minneapolis, MN 55455, USA
[c] Dept. of Mechanical Engineering, University of Minnesota, Minneapolis, MN 55455, USA

ARTICLE INFO

Keywords:
Parietal pleura
Biomechanics
Failure
Uniaxial extension
Lung
Tension pneumothorax

ABSTRACT

Tension pneumothorax, a major preventable cause of battlefield death, often arises from chest trauma and is treated by needle decompression to release trapped air from the pleural cavity. Surgical simulation mannequins are often employed to train medical personnel to perform this procedure properly. Accurate reproduction of the mechanical behavior of the parietal pleura, especially in response to needle penetration, is essential to maximize the fidelity of these surgical simulators. To date, however, the design of pleura-simulating material has been largely empirical and based on subjective practitioner feel rather than on the tissue properties, which have remained unknown. In this study, we performed uniaxial extension tests on samples of cadaveric human parietal pleura. We found that the pleura was highly nonlinear and mildly anisotropic, being roughly twice as stiff in the direction parallel to the ribs vs. perpendicular to the ribs (large-strain modulus = 20.44 vs. 11.49 MPa). We also did not find significant correlations for most pleural properties with age or BMI, but it must be recognized that the age range (59 ± 9.5 yrs) and BMI range (31 ± 5.3) of the donors in our study was not what one might expect from combatants, and there could be differences for younger, lighter individuals. We found a significantly higher low-strain modulus in the diabetic donors (0.213 vs. 0.100 MPa), consistent with the general tendency of tissue to stiffen in diabetes. The nonlinearity and tensile strength should be considered in material design and selection for future surgical simulators.

1. Introduction

Tension pneumothorax (Fig. 1) refers to the progressive buildup of air within the thoracic cavity, often caused by a gunshot wound to the chest. In its most severe cases, the increased pressure may cause a lung to collapse and ultimately lead to traumatic arrest. This condition is associated with 3–4% of total battlefield casualties and is estimated to be the second most common preventable cause of combat-related deaths behind hemorrhage (McPherson et al., 2006; Holcomb et al., 2007; Mabry and McManus, 2008). The standard of care for people suffering from a tension pneumothorax is chest decompression via needle thoracostomy (Beckett et al., 2011; Grabo et al., 2014; Hecker et al., 2016; Lee et al., 2007). In this procedure, a 14–16 G cannula is advanced into the pleural cavity, creating a passage for air to escape. Certified first responders and combat medics are typically trained on this procedure using commercially available surgical simulators (Issenberg, 1999). For example, the TraumaMan® surgical simulator (SIMULAB Corporation, Seattle, WA, USA) allows medical professionals to practice needle decompression, chest tube insertion, and other emergency procedures. These training tools rely on synthetic materials to emulate the different layers of biological tissue found in the thorax. Accurate reproduction of the native tissue properties allows for more realistic training, and is thought to lead to a better performed procedure (Delingette, 1998). For purposes of selecting materials to be used as modeling tissue, manufacturers rely on the qualitative input from experienced practitioners. In particular, the principal requisite for a chosen synthetic to mimic pleural tissue is to capture the characteristic pop that occurs when this membrane is punctured. Current simulators use this qualitative design specification as a guideline for material design, but fail to consider other mechanical properties of the tissue. This failure represents a particular challenge considering that – to the best of the authors' knowledge – there are no data reported on the mechanical properties of human parietal pleura.

The parietal pleura has been studied in other contexts, including electrical resistance (Sarkos et al., 2002), hydraulic conductivity (Negrini et al., 1990), and its role in pleural fluid turnover (Miserocchi, 1997). In addition, the visceral pleura received considerable attention in the 1980s and 90s (Hajji et al., 1979; Stamenovic, 1984; Humphrey

* Corresponding author.
E-mail address: baroc001@umn.edu (V.H. Barocas).

http://dx.doi.org/10.1016/j.jmbbm.2017.07.044
Received 6 May 2017; Received in revised form 21 July 2017; Accepted 28 July 2017
Available online 29 July 2017

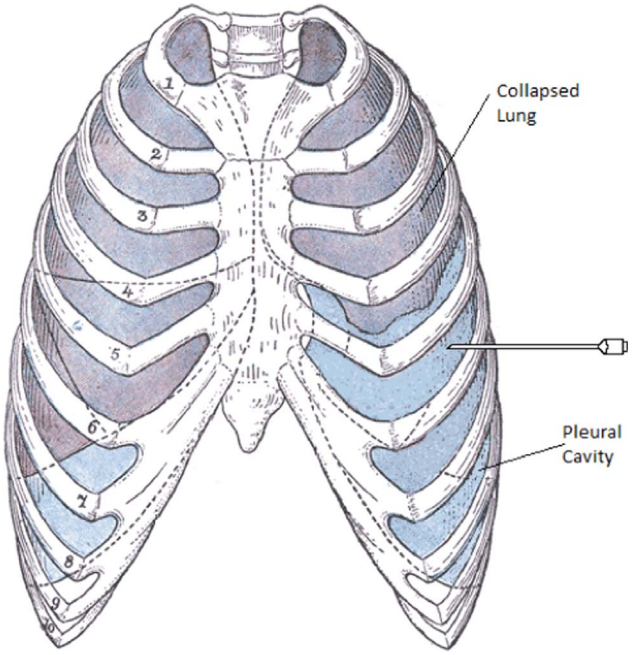

Fig. 1. Tension pneumothorax and needle thoracostomy (adapted from figure 965 of Gray's *Anatomy* (Standring, and Gray, 2008)). The needle is positioned between two ribs and is advanced until it punctures the parietal pleura. This releases the air from the pleural cavity and relieves the pressure on the lung.

et al., 1986, 1987; Humphrey, 1987; Suki et al., 1992) for its role in respiratory mechanics and as a model planar tissue. Visceral pleura was again used as a model planar tissue recently (Freed et al., 2014, 2017), with biaxial extension being employed to characterize the tissue and to evaluate a constitutive framework. The mechanics of the parietal pleura, however, have not been studied. Therefore, it was the goal of this work to study the deformation behavior and mechanical properties of the human cadaveric parietal pleura.

2. Methods

Uniaxial extension to failure experiments were performed on cadaveric pleura samples obtained through American Donor Services (Cottage Grove, MN, USA). Research reported on this publication is IRB-exempt under the code of Federal Regulations part 46 Protection of Human Subjects. Samples were collected from a total of 14 donors (34–70 y/o). A summary of demographic information is shown in Table 1.

2.1. Sample preparation (Fig. 2)

Parietal pleura was dissected and excised from the intercostal muscle. Samples were manually cut into dog-bone shapes approximately 15 mm long and 2 mm wide across the shaft, and dotted with black ink for strain tracking. To test the directionality dependence of the mechanical properties, dog-bones were aligned to two primary directions, parallel to the rib (RIB) and perpendicular to the rib (CROSS). Samples were stored in phosphate-buffered saline until immediately before testing.

2.2. Experimental protocol

Uniaxial extension to failure tests were performed on a TA Instruments TestBench machine (New Castle, DE, USA) with the sample submerged in a temperature-controlled water bath at 37 °C. Samples were pre-conditioned for 5 cycles at 20% strain using a triangular waveform at a frequency of 0.025 Hz. Immediately following preconditioning, samples were pulled to failure at a strain rate of $1\%s^{-1}$ based on the undeformed sample length between the clamps. Testing was video-recorded with a Canon EOS Rebel T6 camera (Melville, NY, USA).

2.3. Data analysis

An in-house image tracking code in Matlab was used to track dots on the tissue during testing. The stretch ratio (λ) was calculated based on the movement of these dots. Using the initial dimensions of each sample, the 1st Piola Kirchhoff stress (*PK1*) was computed, and stress-stretch curves were generated. Six characteristic parameters were analyzed, as shown in Fig. 3. The ultimate tensile stress (*UTS*) and the stretch at failure (λ_{max}) were defined by the point where the sample failed. Strain energy density (W) was defined as the area under the stress-stretch curve and represented the amount of energy required to stretch the sample to failure. Following previous studies (Babu et al., 2015; Freed et al., 2016; Jones et al., 2009; Skelley et al., 2015), we used a bilinear fit to analyze the data and determined two moduli and a transition point. The high-strain tangent modulus E_2 was taken as the slope of the linear portion of the curve fitted between 30–70% of the UTS. The low-strain tangent modulus E_1 was taken as the slope of the toe region of the curve ($\leq$ 1% of UTS). The transitional stretch (λ_t) was defined as the stretch at which the two linear fits intercepted. All six parameters were compared between the two directions of interest (i.e. RIB vs CROSS), and over the other relevant demographic information (i.e. age, BMI, smoker vs. non-smoker, diabetic vs. non-diabetic).

Table 1
Donor demographics. The columns *n CROSS* and *n RIB* give the number of samples perpendicular to and parallel to the ribs obtained for each donor, respectively.

Donor	Gender	Age	BMI	Diabetic	Smoker	n CROSS	n RIB
A	Male	34	22	–	–	0	8
B	Female	59	37	–	+	3	1
C	Male	54	33	–	+	4	0
D	Male	56	37	–	–	5	1
E	Male	55	27	–	+	3	1
F	Male	70	34	+	+	1	3
G	Male	67	39	+	+	6	9
H	Male	62	32	–	–	3	3
I	Female	57	30	–	+	2	1
J	Male	69	31	+	+	4	2
K	Male	70	32	+	–	4	3
L	Male	63	23	–	–	1	2
M	Male	53	29	–	–	1	3
N	Male	53	25	–	+	1	1
Total/Mean ± SD	M(12)/F(2)	59 ± 9.5	31 ± 5.3	4(+)/10(-)	8(+)/6(-)	38	38

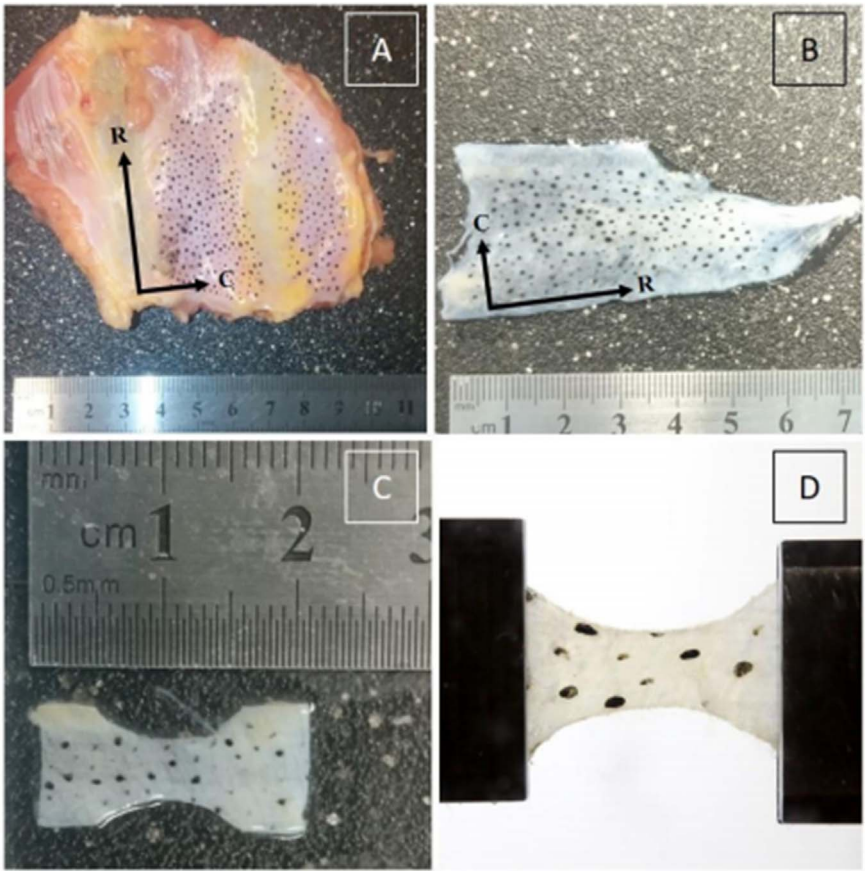

Fig. 2. Sample preparation. A) Entire intercostal section with intact skin, adipose tissue, intercostal muscle, ribs, and parietal pleural membrane. B) Blunt dissection of parietal pleural membrane with waterproof black ink dotting. C) Dog-bone sample cut from the large tissue sample in (B). D) Gripped dog-bone sample mounted on TA Electroforce TestBench instrument for uniaxial extension to failure.

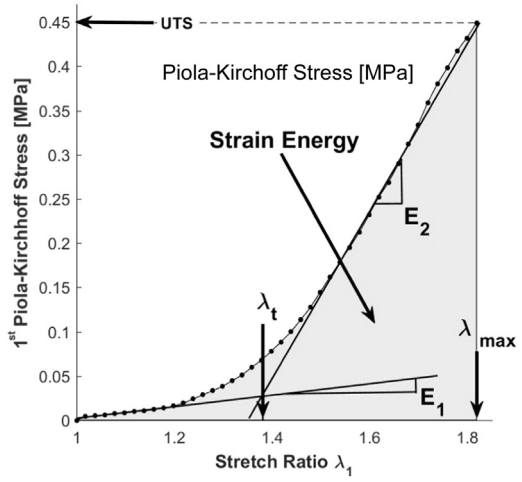

Fig. 3. Quantitative measurements of mechanical behavior. The low-strain modulus (E_1) and the high-strain modulus (E_2) were calculated by fitting lines to the stress-stretch curve, with their intersection defining the transition stretch (λ_t). The ultimate tensile stress (UTS) and stretch at failure (λ_{max}) were also calculated, as well as the strain energy (W), i.e., the integral of the λ-S curve.

2.4. Statistical analysis

In order to test the directionality dependence of the parameters studied, all samples aligned in a given direction for each donor were lumped, and subsequently a paired *t*-test was performed between CROSS and RIB samples for all donors from whom both types had been obtained (n = 12). For continuous-variable demographic information, i.e. age and BMI, a linear regression between each mechanical parameter and these variables was computed, and the p-value for the null hypothesis of zero slope was computed. The effect of binary demographic information (tobacco use and diabetes) was also subjected to a statistical analysis. A *t*-test was performed for donors who were reported as smokers (n = 8) vs. non-smokers (n = 6) and for diabetic (n = 4) vs. non-diabetic (n = 10) donors.

3. Results

Fig. 4 shows typical stress-stretch curves for samples in the RIB and CROSS directions. Like most soft tissues, the parietal pleura samples showed a low-stiffness toe region followed by a transition to greater

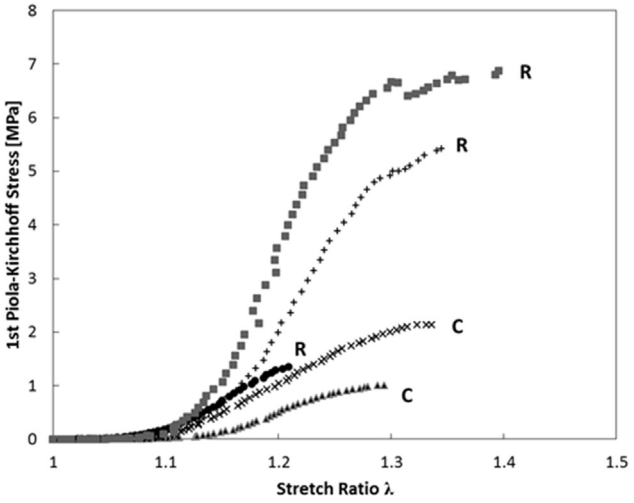

Fig. 4. Representative data of five samples for the same donor. C = CROSS, R = RIB. Data are only shown up to the peak stress.

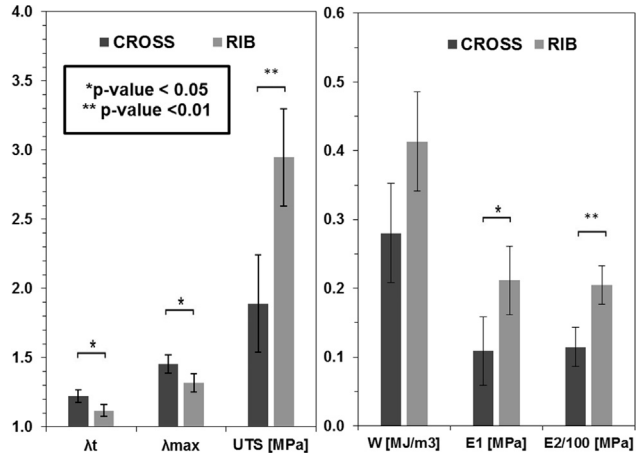

Fig. 5. Paired *t*-test results comparing the mechanical properties of pleura tissue in the CROSS and RIB directions. The two directions showed significantly different properties with the transition stretch (λ_t), the maximum stretch (λ_{max}), and the low-strain modulus (E_1) having p-values of < 0.05, and the ultimate tensile strength (UTS) and high–strain modulus (E_2) having p-values of < 0.01. This indicates pleura tissue is more rigid in the direction of the ribs.

stiffness and finally failure.

As can be seen in Fig. 5, the comparison between the CROSS and RIB directions yielded statistically significant differences ($p < 0.05$) for five of the six quantities studied (all except strain energy), indicating significant anisotropy in the tissue. Specifically, samples aligned in the CROSS direction showed longer toe regions ($\lambda_t = 1.22$ vs. 1.12), larger failure stretches ($\lambda_{max} = 1.45$ vs. 1.32), and lower ultimate tensile strength (UTS = 1.89 vs. 2.95 MPa). The stiffness of the tissue was also lower in the CROSS direction, both in the low-strain ($E_1 = 0.11$ vs. 0.21 MPa) and the high-strain ($E_2 = 11.49$ vs. 20.44 MPa) regimes. Taken together, these indicate that the tissue is more compliant, more distensible, and less strong in the CROSS direction than in the RIB direction.

Plotting the properties vs. age (Fig. 6) showed a significant relationship between age and the low-strain modulus E_1 ($p = 0.047$). The rest of the plots showed no significant trends, with R^2 values all less than 0.21 and p-values all greater than 0.1. It is notable that the tissue from a 34-year old donor had low UTS, modulus, and strain energy when compared to tissue from the other donors, who were aged 53–70. Although it is not possible to draw statistically meaningful conclusions from this single data point, and the age range of donor tissue tends to skew towards older individuals, the 34-year-old data point merits further investigation. The question of age dependence is further emphasized by the relative youth of military combatants. There was also no significant change in properties with BMI (Fig. 7); no effect of BMI was expected, but this result is again important in light of the fact that soldiers tend to be quite trim.

We saw no significant changes to the tissue properties between the smoker and non-smoker groups (Fig. 8a and b), but there were differences between the diabetic and non-diabetic groups (Fig. 8c and d), some of which were significant at the 95% confidence level. Specifically, the diabetic tissue was stiffer ($E_1 = 0.21$ vs. 0.10 MPa, $p = 0.039$; $E_2 = 19.15$ vs. 12.02 MPa, $p = 0.167$), stronger (UTS = 2.96 vs. 1.84 MPa, $p = 0.18$), and had a shorter toe region ($\lambda_t = 0.47$ vs. 1.24, $p = 0.00025$) when compared to the non-diabetic tissue.

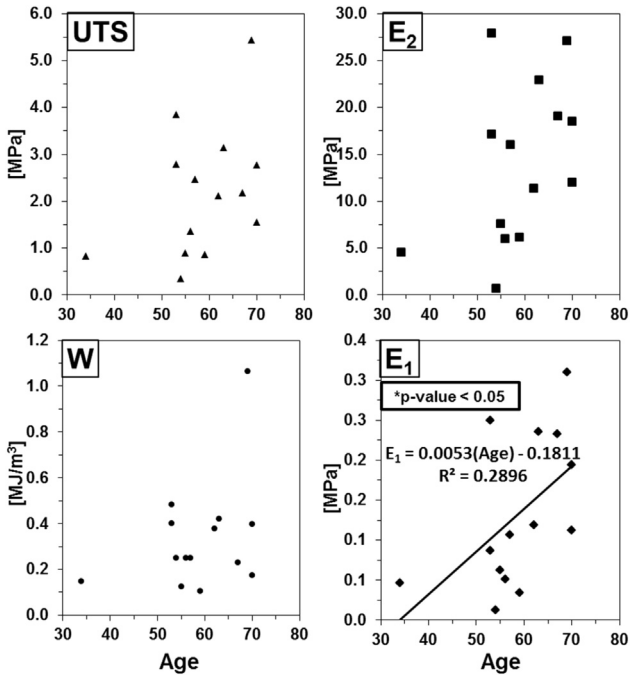

Fig. 6. Linear regression of mechanical parameters vs Age [years]. The data showed a significant relationship between the low-strain modulus (E_1) and age, with a p-value of 0.047. This suggests the stiffening of pleura in the low-strain regime with age. All other parameters showed no significant relationship with age. On average, soldiers are 21.6 years old when they enter the US Army (Hruby et al., 2017). Only E_1 gave a linear fit with a slope significantly different from zero ($p < 0.05$).

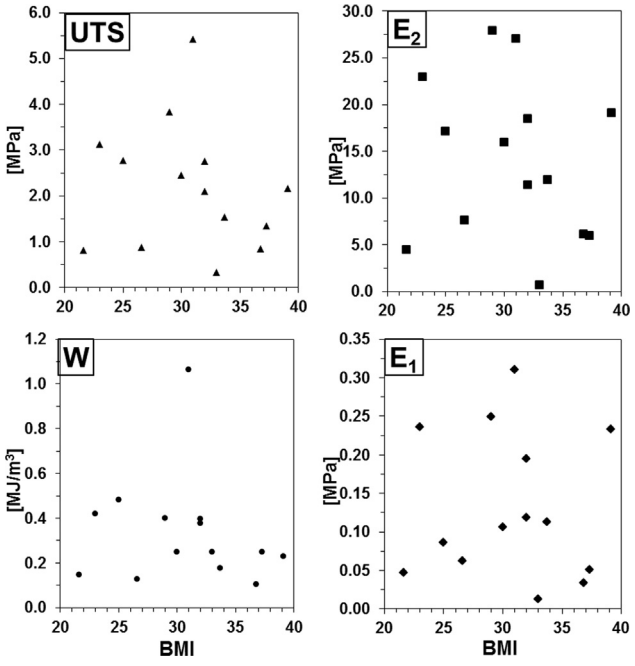

Fig. 7. Linear regression of mechanical parameters vs BMI. No relationship between the mechanical parameters and BMI was observed from the data. All parameters had p-values > 0.6. 55.9% of soldiers are considered to be underweight or of normal weight (BMI < 25) and 34.2% of soldiers are considered to be overweight ($25 \leq$ BMI < 30) when entering the US Army (Hruby et al., 2017).

4. Discussion

The major result of this study is the quantification of the mechanical properties of the human parietal pleura, which is particularly relevant to surgical simulator design (Berkenstadt et al., 2006; Davis et al., 2012). Current simulators include a variety of materials to replicate the parietal pleura including viscoelastic foam impregnated with silicone or latex (Buckman, 2009), nylon mesh coated with silicone (Toly, 2004), and layered latex and fabric (Dawson et al., 2004). The results of this study will help define a standard for parietal pleura synthetics for future surgical models.

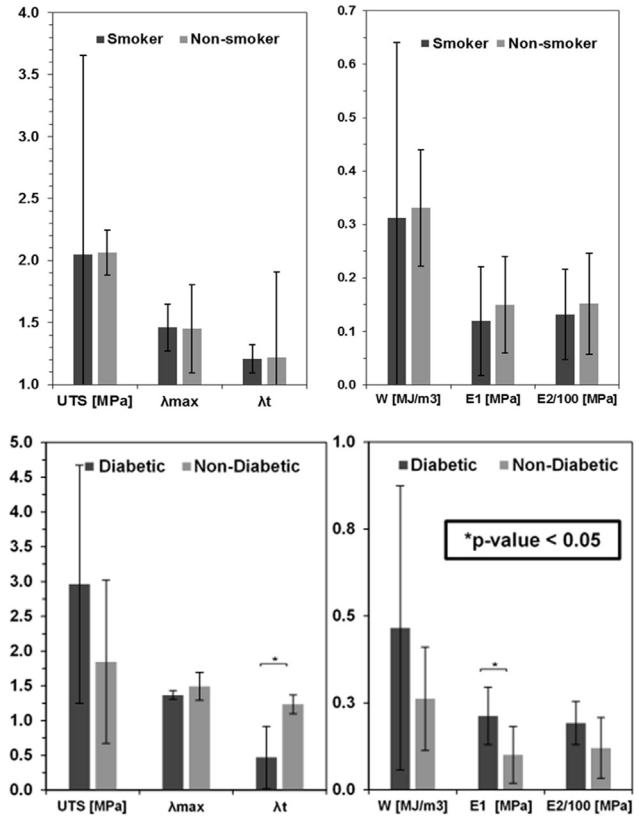

Fig. 8. Statistical analysis of binary data. Top row displays the results of the *t*-tests comparing the mechanical properties of Smoker vs non-Smoker donors. The bottom row displays the results of the *t*-tests comparing Diabetic vs non-Diabetic donors. No relationship was observed between the mechanical parameters and the tobacco use of the donors. These comparisons had p-values > 0.5. Significant relationships were observed between diabetes, the low-strain modulus (E_1), and the transitional stretch (λ_t). These comparisons had p-values < 0.04.

We found the parietal pleura to be highly nonlinear ($E_2 \approx 100X\ E_1$) and moderately anisotropic (roughly twice as stiff parallel to the ribs), which is consistent with observations made about a number of different collagenous tissues (see (Fung, 2010) or any other good tissue mechanics text). While the significance of the anisotropy is not clear, the nonlinearity undoubtedly affects the practitioner's experience during needle insertion and should be considered in the materials selection for future surgical simulators. It may prove advantageous to use a membrane model such as (Freed et al., 2014) to model the mechanical behavior of the parietal pleura, with appropriate modification to account for tissue anisotropy. Other structural models (e.g., Bellini et al., 2016; Billiar et al., 1997; Gasser et al., 2006; Holzapfel et al., 2000; Ramesh et al., 2009) could also be applied.

We found almost no correlation in properties with age or BMI. This result is important given that a majority of soldiers are young and have a BMI below 25 (Hruby et al., 2017), but tissue donors tend to be older (59 ± 9.5 years old in this study) and more overweight (BMI $= 31 \pm 5.3$). Our donor range was far enough removed from the typical soldier range, however, that care should still be taken in using our data. There was no correlation with age or BMI over the range studied, but there could be differences in parietal properties in significantly younger and fitter adults. The lack of effect of smoking was expected since the parietal pleura does not contact inhaled air, but we considered it an important test because smoking has such profound effects on lung biology.

The significant effect of diabetes was interesting and merits further study. Diabetes is well known to lead to stiffening of arteries and other collagenous tissues throughout the body (Yang et al., 2004; Fields et al., 2015; Yang et al., 2017), so one might expect to see stiffening of the parietal pleura as well, but we believe that this is the first study in which the effect of diabetes on parietal pleura stiffness was reported. There is no indication that the stiffening has functional consequences.

The results of this study could also be relevant to the improvement of finite-element injury models, which generally lump the parietal pleura in with the surrounding soft tissue rather than treating it as a separate mechanical element (Niu et al., 2008; Gibbons et al., 2015; Danelson and Stitzel, 2015; Hayes et al., 2014). Some vehicular impact models use morphomic variables, such as body fat and muscle composition, to predict thoracic injuries (Zhang et al., 2013). The addition of parietal pleura to these models could improve the accuracy of the injury predictions.

Acknowledgements

The authors thank the anonymous donors whose tissue was used in this study. Research was sponsored in part by the Army Research Laboratory and was accomplished under Cooperative Agreement Number W911NF-14-2-0035. The views and conclusions contained in this document are those of the authors and should not be interpreted as representing the official policies, either expressed or implied, of the Army Research Laboratory or the U.S. Government. The U.S. Government is authorized to reproduce and distribute reprints for Government purposes notwithstanding any copyright notation herein.

References

Babu, A.R., Byju, A.G., Gundiah, N., 2015. Biomechanical properties of human ascending thoracic aortic dissections. J. Biomech. Eng. 137 (8), 081013.
Beckett, A., Savage, E., Pannell, D., Acharya, S., Kirkpatrick, A., Tien, H.C., 2011. Needle decompression for tension Pneumothorax in tactical combat casualty care: do catheters placed in the midaxillary line Kink more often than those in the midclavicular line? J. Trauma.: Inj. Infect. Crit. Care 71, S408–S412.
Bellini, C., Korneva, A., Zilberberg, L., Ramirez, F., Rifkin, D.B., Humphrey, J.D., 2016. Differential ascending and descending aortic mechanics parallel aneurysmal propensity in a mouse model of Marfan syndrome. J. Biomech. 29, 2383–2389.
Berkenstadt, H., Munz, Y., Trodler, G., Blumenfeld, A., Rubin, O., Ziv, A., 2006. Evaluation of the trauma-man simulator for training in chest drain insertion. Eur. J. Trauma 32, 523–526.
Billiar, K.L., Sacks, M.S., 1997. A method to quantify the fiber kinematics of planar tissues under biaxial stretch. J. Biomech. 30 (7), 753–756.
Buckman, R.F., 2009. U.S. Patent No. 20090246747 A1. U.S. Patent and Trademark Office, Washington, DC.
Danelson, K.A., Stitzel, J.D., 2015. Finite element model prediction of pulmonary contusion in vehicle-to-vehicle simulations of real-world crashes. Traffic Inj. Prev. 16 (6), 627–636.
Davis, J.S., Garcia, G.D., Wyckoff, M.M., Alsafran, S., Graygo, J.M., Withum, K.F., Schulman, C.I., 2012. Use of mobile learning module improves skills in chest tube insertion. J. Surg. Res. 177, 21–26.
Dawson, S., Ottensmeyer, M., Cotin, S., Newmann, P., 2004. U.S. Patent No. 20040234933 A1. U.S. Patent and Trademark Office, Washington, DC.
Delingette, H., 1998. Toward realistic soft-tissue modeling in medical simulation. Proc. Ieee. 86 (3), 512–523.
Fields, A.J., Berg-Johansen, B., Metz, L.N., Miller, S., La, B., Liebenberg, E.C., Coughlin, D. G., Graham, J.L., Stanhope, K.L., Havel, P.J., Lotz, J.C., 2015. J. Orthop. Res.
Freed, A.D., Erel, V., Moreno, M.R., 2017. Conjugate stress/strain base pairs for the analysis of planar biologic tissues. J. Mech. Mater. Struct. 12, 219–247.
Freed, A.D., Liao, J., Einstein, D.R., 2014. A membrane model from implicit elasticity theory: application to visceral pleura. Biomech. Model. Mechanobiol. 13, 871–881.
Freed, A.D., Rajagopal, K.R., 2016. A promising approach for modeling biological fibers. Acta Mech. 227, 1609–1619.
Fung, Y.C., 2010. Biomechanics: Mechanical Properties of Living Tissues, 2nd ed. SpringerVerlag New York, New York.
Gasser, T.C., Ogden, R.W., Holzapfel, G.A., 2006. Hyperelastic modelling of arterial layers with distributed collagen fibre orientations. J. R. Soc. Interface 3, 15–35.
Gibbons, M.M., Dang, X., Adkins, M., Powell, B., Chan, P., 2015. Finite element modeling of blast lung injury in sheep. J. Biomech. Eng. 137.
Grabo, D., Inaba, K., Hammer, P., Karamanos, E., Skiada, D., Martin, M., Sullivan, M., Demetriades, D., 2014. Optimal training for emergency needle thoracostomy placement by prehospital personnel. J. Trauma Acute Care Surg. 77, S109–S113.
Hajji, M.A., Wilson, T.A., Lai-Fook, S.J., 1979. Improved measurements of shear modulus and pleural membrane tension of the lung. J. Appl. Physiol. 47 (1), 175–181.
Hayes, A.R., Valvalle, N.A., Moreno, D.P., Stitzel, J.D., Gayzik, F.S., 2014. Validation of simulated chestband data in frontal and lateral loading using a human body finite element model. Traffic Inj. Prev. 15 (2), 181–186.
Hecker, M., Hegenscheid, K., Völzke, H., Hinz, P., Lange, J., Ekkernkamp, A., Frank, M.,

2016. Needle decompression of tension pneumothorax. J. Trauma Acute Care Surg. 80, 119–124.
Holcomb, J.B., McMullin, N.R., Pearse, L., Caruso, J., Wade, C.E., Oetjen-Gerdes, L., Champion, H.R., Lawnick, M., Farr, W., Rodriguez, S., Butler, F.K., 2007. Causes of death in U.S. Special operations forces in the global war on terrorism. Ann. Surg. 245, 986–991.
Holzapfel, G.A., Gasser, T.C., Ogden, R.W., 2000. A new constitutive framework for arterial wall mechanics and a comparative study of material models. J. Elast. 61, 1–48.
Hruby, A., Bulathsinhala, L., McKinnon, C.J., Hill, O.T., Montain, S.J., Young, A.J., Smith, T.J., 2017. Body mass index at accession and incident cardiometabolic risk factors in US army soldiers, 2001–2011. PLOS ONE.
Humphrey, J.D., 1987. A possible role of the pleura in lung mechanics. J. Biomech. 20, 773–777.
Humphrey, J.D., Vawter, D.L., Vito, R.P., 1986. Mechanical behavior of excised canine visceral pleura. Ann. Biomech. Eng. 14, 451–466.
Humphrey, J.D., Vawter, D.L., Vito, R.P., 1987. Pseudoelasticity of excised visceral pleura. J. Biomech. Eng. 109, 115.
Issenberg, S.B., 1999. Simulation technology for health care professional skills training and assessment. JAMA 282, 861.
Jones, K.A., Feola, A., Meyn, L., Abramowitch, S.D., Moalli, P.A., 2009. Tensile properties of commonly used prolapse meshes. Int. Urogynecol. J. 20, 847–853.
Lee, C., Revell, M., Porter, K., Steyn, R., 2007. The prehospital management of chest injuries: a consensus statement. faculty of pre-hospital care, royal college of surgeons of Edinburgh. Emerg. Med. J. 24, 220–224.
Mabry, R., McManus, J.G., 2008. Prehospital advances in the management of severe penetrating trauma. Crit. Care Med. 36, S258–S266.
McPherson, J.J., Feigin, D.S., Bellamy, R.F., 2006. Prevalence of tension pneumothorax in fatally wounded combat casualties. J. Trauma.: Inj. Infect. Crit. Care 60, 573–578.
Miserocchi, G., 1997. Physiology and pathophysiology of pleural fluid turnover. Eur. Respir. J. 10, 219–225.
Negrini, D., Townsley, M.I., Taylor, A.E., 1990. Hydraulic conductivity of canine parietal pleura in vivo. J. Appl. Physiol. 69 (2), 438–442.
Niu, W.S.Y., Mattrey, R.F., Fournier, A., Kono, J.C.Y., Stuhmiller, J.H., 2008. Development and validation of subject-specific finite element models for blunt trauma study. J. Biomech. Eng. 130.
Ramesh, R., Barocas, V.H., 2009. A closed-form structural model of planar fibrous tissue mechanics. J. Biomech. 42 (10), 1424–1428.
Sarkos, S., Hatzoglou, C., Dahabre, J., Gourgoulianis, K.I., Molyvdas, P.A., 2002. Effect of amiloride in human and sheep parietal pleura. Respir. Physiol. Neurobiol. 132 (2), 233–237.
Skelley, N.W., Castile, R.M., York, T.E., Gruev, V., Lake, S.P., Brophy, R.H., 2015. Differences in the microstructural properties of the anteromedial and posterolateral bundles of the anterior cruciate ligament. Am. J. Sports Med. 43 (4), 928–936.
Stamenovic, D., 1984. Mechanical properties of pleural membrane. J. Appl. Physiol. 57 (4), 1189–1194.
Standring, S., Gray, H., 2008. Gray's Anatomy: the Anatomical Basis of Clinical Practice. Churchill Livingstone/Elsevier, Edinburgh.
Suki, B., Hantos, Z., 1992. Viscoelastic properties of visceral pleura and its contribution to lung impedance. Respir. Physiol. 90, 271–287.
Toly, C.C., 2004. U.S. Patent No. 6780016 B1. U.S. Patent and Trademark Office, Washington, DC: .
Yang, J., Zhao, J., Zeng, Y., Gregersen, H., 2004. Biomechanical properties of the rat oesophagus in experimental type-1 diabetes. Neurogastroenteral Motil. 16, 195–203.
Yang, X., Scott, H.A., Monickaraj, F., Xu, J., Ardekani, S., Nitta, C.F., Cabrera, A., McGuire, P.G., Mohideen, U., Das, A., Ghosh, K., 2017. Basement membrane stiffening promotes retinal endothelial activation associated with diabetes. FASEB J. 30 (2), 601–611.
Zhang, P., Parenteau, C., Holcombe, S., Kohoyda-Inglis, C., Sullivan, J., Wang, S., 2013. Prediction of thoracic injury severity in frontal impacts by selected anatomical morphomic variables through model-averaged logistic regression approach. Accid. Anal. Prev. 60, 172–180.